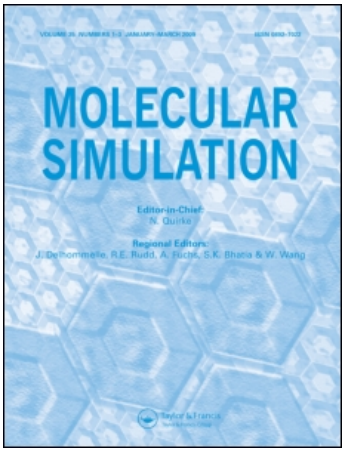

Molecular Simulation
Publication details, including instructions for authors and subscription information:
http://www.informaworld.com/smpp/title~content=t713644482

Crystallographic phase stabilities and electronic structures in $AgNbO_3$ by first-principles calculation

Akio Shigemi[a]; Takahiro Wada[a]
[a] Department of Materials Chemistry, Wada Laboratory, Ryukoku University, Otsu, Japan

To cite this Article Shigemi, Akio and Wada, Takahiro(2008) 'Crystallographic phase stabilities and electronic structures in $AgNbO_3$ by first-principles calculation', Molecular Simulation, 34: 10, 1105 — 1114
To link to this Article: DOI: 10.1080/08927020802235698
URL: http://dx.doi.org/10.1080/08927020802235698

Molecular Simulation
Vol. 34, Nos. 10–15, September–December 2008, 1105–1114

Taylor & Francis
Taylor & Francis Group

Crystallographic phase stabilities and electronic structures in $AgNbO_3$ by first-principles calculation

Akio Shigemi* and Takahiro Wada[1]

Department of Materials Chemistry, Wada Laboratory, Ryukoku University, Otsu, Japan

(*Received 31 January 2008; final version received 27 May 2008*)

Silver niobate ($AgNbO_3$) assumes several phases that crystallise in the perovskite structure similar to sodium niobate ($NaNbO_3$). In order to investigate the phase stability of $AgNbO_3$, the formation enthalpies of both physically the realised (real) cubic ($Pm\bar{3}m$), tetragonal ($P4/mbm$) and orthorhombic ($Cmcm$, $Pbcm$) phases as well as the virtual phases, the orthorhombic ($Pc2_1b$) and rhombohedral ($R3cR$) phases, which are observed in $NaNbO_3$, have been obtained using a plane-wave pseudopotential method. Although the orthorhombic ($Pbcm$) phase has the lowest formation enthalpy among the real phases, the virtual rhombohedral ($R3cR$) phase has the lowest symmetry as well as the lowest formation enthalpy among all phases. We thus speculate that the rhombohedral ($R3cR$) phase may be stable at extremely low temperatures provided that it is accessible kinetically. In addition, the electronic structures of the various phases of $AgNbO_3$ are calculated within the generalised gradient approximation with the Perdew–Burke–Ernzerhof correction (GGA-PBE). The valence band top was found to consist of predominately localised Ag 4d and O 2p orbitals constituting the O 2p—Nb 4d bonding orbital, while the bottom of the conduction band was found to mainly consist of the anti-bonding orbital of Nb 4d—O 2p under the Ag 5s orbital.

Keywords: $AgNbO_3$; first-principles pseudopotential calculation; formation enthalpy; phase stability; electronic structure

1. Introduction

To date, we have primarily used $Pb(Zr,Ti)O_3$ (PZT) as piezoelectric materials. Piezoelectric ceramics have been used for various applications [1], e.g. pressure sensors, accelerometers, piezoelectric vibrators, ultrasonic transducers, piezoelectric transformers, piezoelectric actuators, ultrasonic motors, etc. Recently, lead-free piezoelectric ceramic materials have come under the spotlight from the viewpoint of environmental protection. $ANbO_3$ (A = Li, Na and K) has been studied as a candidate for a lead-free piezoelectric material that can replace PZT. Saito et al. [2] reported that $(Li,Na,K)(Nb,Ta,Sb)O_3$ solid solution ceramics showed strong piezoelectric features ($d_{33} > 300$ pC/N) and a high Curie temperature ($T_c > 200$°C) comparable to the values of PZT ceramics [2]. After this pioneering work, many research groups have searched for new piezoelectric materials in the niobate system. We have theoretically studied the $ANbO_3$ (A = Li, Na and K) system [3–6] using a plane-wave pseudopotential method (CASTEP code) [7] within the generalised gradient approximation with the Perdew–Burke–Ernzerhof correction (GGA-PBE) [8] of density functional theory. It is known that $LiNbO_3$ and $KNbO_3$ exhibit piezoelectricity, $NaNbO_3$ is anti-ferroelectric at room temperature. Among the stabilised phases of $ANbO_3$ at atmosphere pressure, $LiNbO_3$ shows the only structural phase transition between a paraelectric and ferroelectric phase (at 1210°C), but $NaNbO_3$ and $KNbO_3$ show a number of structural phase transitions between a paraelectric cubic and ferroelectric rhombohedral phase [9].

In a previous study, we evaluated the formation enthalpies of the various $NaNbO_3$ phases [3,5] using a first-principle calculation [7]. The formation enthalpies obtained for the various phases, e.g. cubic ($Pm\bar{3}m$), tetragonal ($P4/mbm$), orthorhombic ($Ccmm$, $Pnmm$, $Pbma$) and rhombohedral ($R3cR$) phases, decrease with decreasing crystal symmetry, and the lowest symmetry rhombohedral ($R3cR$) phase was found to have the lowest formation enthalpy. This result corresponded to the experimental result that the rhombohedral phase was stable at ultra low temperatures.

$Ag(Nb_{1-x}Ta_x)O_3$ ceramics have been investigated as microwave dielectrics [10]. $AgNbO_3$ in the perovskite structure shows weak ferroelectricity at room temperature and undergoes several phase transitions with temperature. Initially, its ferroelectricity was studied by Francombe and Lewis [11], and its crystallographic and dielectric properties were studied by others [11–14]. The space groups for calcined $AgNbO_3$ powder were also analysed from 24 to 630°C. Pure $AgNbO_3$ undergoes successive phase transitions from the ferroelectric orthorhombic phase ($Pbcm$) to the paraelectric orthorhombic phase ($Cmcm$) at 347°C, then to tetragonal phase ($P4/mbm$) at 377°C, and finally to the cubic phase ($Pm\bar{3}m$) at 530°C [15].

*Corresponding author. Email: shigemi@project1.hrc.ryukoku.ac.jp

ISSN 0892-7022 print/ISSN 1029-0435 online

DOI: 10.1080/08927020802235698
http://www.informaworld.com

More recently, Fu et al. [16] found that a new antiferroelectric state in $AgNbO_3$ phase appears under high electric fields (over 110 kV/cm) at room temperature [16]. Lithium-doped silver niobate (Ag, Li) NbO_3 has also been studied [14,17,18]. (Ag,Li)NbO_3 shows ferroelectric behaviour at room temperature and has several phases with different compositions. For calcined $(Ag_{0.9}Li_{0.1})$-NbO_3 powder, the space groups of the prepared material were analysed as well as those of $AgNbO_3$ by Wada et al. [18]. We believe that the properties of $AgNbO_3$ are very similar to those of $NaNbO_3$.

In this study, we evaluate the formation enthalpies of the various $AgNbO_3$ phases using a plane-wave pseudopotential method to investigate the phase stabilities for all of the experimentally confirmed $AgNbO_3$ phases ($Pm\bar{3}m$, $P4/mbm$, $Cmcm$ and $Pbcm$) that occur at atmospheric pressure and for the virtual phases ($Pc2_1b$ and $R3cR$), which are observed in $NaNbO_3$. The model structures of these phases were constructed on the basis of the experimental crystal structural data of $AgNbO_3$ and $NaNbO_3$ (see the footnote in Table 1). The formation enthalpies of the various $AgNbO_3$ phases were obtained by the first-principles calculation. Additionally, we have investigated the electronic structure of the various $AgNbO_3$ phases, and discuss these results in comparison with the electronic structures of $NaNbO_3$.

2. Computational procedures

All calculations were carried out within the GGA-PBE [8,25] of density functional theory, using a plane-wave pseudopotential method (CASTEP code) [7]. A *k*-point mesh generated by the Monkhorst–Pack scheme [19] was employed for numerical integrations over the Brillouin zone. The $6 \times 6 \times 6$, $4 \times 4 \times 6$, $3 \times 3 \times 3$, $4 \times 4 \times 2$, $5 \times 2 \times 4$ and $3 \times 3 \times 3$ *k*-point meshes were used for the cubic ($Pm\bar{3}m$), tetragonal ($P4/mbm$), orthorhombic ($Cmcm$), orthorhombic ($Pbcm$), orthorhombic ($Pc2_1b$) and rhombohedral ($R3cR$) phases of $AgNbO_3$, respectively. Ultrasoft pseudopotentials [20] were applied with a plane-wave cutoff energy of 410 eV. The convergence of the total energies with respect to the cutoff energy at 600 eV was better than 0.05 eV for $AgNbO_3$.

The self-consistent total energies were obtained using the Pulay method for the density mixing scheme [21] in connection with the conjugate gradient technique [22]. Calculations for geometry optimisations were performed with symmetry restriction. Atomic positions and lattice parameters were optimised by means of the quasi-Newton method with the Broyden–Fletcher–Goldfarb–Shanno scheme [23]. The tolerances of total energy convergence, max-ionic force, max-ionic displacement and max-stress component were 5×10^{-6} eV/atom, 1×10^{-2} eV/Å, 5×10^{-4} Å and 2×10^{-2} GPa, respectively. We also performed calculations for many reference materials, i.e. Ag (cubic: $Fm\bar{3}m$), Nb (cubic: $Im\bar{3}m$), crystalline O_2 (monoclinic: $C2/m$), Ag_2O (cubic: $Fm\bar{3}m$), NbO (cubic: $Pm\bar{3}m$), NbO_2 (tetragonal: $I41/aZ$) and Nb_2O_5 (monoclinic: $A2/m$). We utilised a O_2 molecular crystal, i.e. antiferromagnetic α-solid O_2 [24], as our model structure, although experimental data were generally defined not by solid O_2 with a $C2/m$ structure but by O_2 (gas) as a standard. Spin polarisation was taken into consideration for the ground state O_2 (triplet). The theoretical lattice parameter of O_2 was fixed to the experimental value. The total energies of the reference materials were obtained after the structures were optimised by the same computational method for consistency.

Table 1. Lattice parameters of the various $AgNbO_3$ phases.

		Lattice parameters (Å)		
Crystal system	Space group	Theoretical	Experimental	Error (%)
Cubic	$Pm\bar{3}m$	$a = 3.979$	$a = 3.960$[a]	+0.5
Tetragonal	$P4/mbm$	$a = 5.564$	$a = 5.582$[b]	−0.3
		$c = 3.978$	$c = 3.960$	+0.5
Orthorhombic	$Cmcm$	$a = 7.843$	$a = 7.883$[c]	−0.5
		$b = 7.894$	$b = 7.890$	+0.1
		$c = 7.924$	$c = 7.906$	+0.2
Orthorhombic	$Pbcm$	$a = 5.602$	$a = 5.544$[d]	+1.0
		$b = 5.692$	$b = 5.607$	+1.5
		$c = 15.601$	$c = 15.565$	+0.2
Orthorhombic	$Pc2_1b$ [VP]	$a = 5.543$		
		$b = 15.905$		
		$c = 5.648$		
Trigonal/rhombohedral	$R3cR$ [VP]	$a = 7.935$		
		$\alpha = 88.856°$		

VP: Virtual phase.
[a] ICSD #55649 (903 K). [b] ICSD #55648 (733 K). [c] ICSD #55647 (645 K). [d] ICSD #55643 (1.5 K, 573 K: ICSD #55646).

Calculations for electronic structures were also performed using the GGA-PBE exchange-correlation functional [8,25]. The band structures and densities of states (DOS) for various $AgNbO_3$ phases were obtained under the same calculation condition. For the sake of the comparison, the electronic structures of various $NaNbO_3$ phases were also calculated.

3. Results and discussion

3.1 Crystallographic characterisation of $AgNbO_3$

3.1.1 Lattice parameters

The lattice parameters of the various $AgNbO_3$ phases are tabulated in Table 1. The theoretically calculated lattice parameters for the various $AgNbO_3$ phases were obtained at 0 K, and in contrast, the experimental values were obtained at higher temperatures. The theoretical lattice parameters for $AgNbO_3$ calculated using the above procedure, however, were consistent with the corresponding experimental values within an error of $\pm 2\%$, a typical error value for density functional calculations. The model structures of the virtual $Pc2_1b$ and $R3cR$ phases of $AgNbO_3$ were constructed on the basis of the experimentally determined structural data of $NaNbO_3$ [26,27]. The theoretical values of a, b and c for the orthorhombic ($Pc2_1b$) phase of $AgNbO_3$ were 5.543, 15.905 and 5.648 Å, respectively. These values approximate the experimental values of 5.494, 15.461 and 5.551 Å for $NaNbO_3$ ([26], inorganic crystal structure database (ICSD)#38314). The theoretical values for rhombohedral ($R3cR$) phase in $AgNbO_3$ were also found to be in reasonable agreement with the experimental values of 7.8147 Å and 89.17° for $NaNbO_3$ ([27], ICSD#9645). In addition, considering that the ionic radius of eight-coordinated Ag^+(= 128 pm; Ag^+ in the A-site of the perovskite structure is actually surrounded by 12 oxygen ions) is approximately equivalent to that of eight-coordinated Na^+(= 118 pm) [28], we speculate that the optimised virtual phases in $AgNbO_3$ are reliable crystal structures.

For completeness, the lattice parameters of the reference materials are summarised in Table 2. The theoretical values of the lattice parameters of the reference materials also correspond to their experimental values within an error of $\pm 2\%$.

3.1.2 Interatomic distances and distortion angles in various phases

The spontaneous polarisation depends on both the displacement magnitude from the symmetry centre and the Born effective charge. Therefore, it is worth examining the distortion effect of $AgNbO_3$. We examined unit cell distortion for the $AgNbO_3$ structure with decreasing unit cell symmetry. Bond angles and interatomic distances of various $AgNbO_3$ phases are shown in Table 3. $AgNbO_3$ in the cubic ($Pm\bar{3}m$) phase assumes the ideal perovskite structure without distortion (refer to Figure 1). $AgNbO_3$ in the tetragonal ($P4/mbm$) phase gives rise to a two-dimensional distortion of the oxygen octahedron in the direction towards the *X*- and *Y*-axes, and short and long bond lengths occur in the interatomic spacings of Nb—O and Ag—O. $AgNbO_3$ in the orthorhombic ($Cmcm$, $Pbcm$,

Table 2. Lattice parameters of reference materials for $AgNbO_3$.

Compounds	Crystal system (space group)	Lattice parameters (Å)		Error (%)
		Theoretical	Experimental	
Ag_2O	Cubic ($Pn\bar{3}mS$)	$a = 4.806$	$a = 4.76$[a]	+1.0
Nb_2O_5	Monoclinic ($A2/m$)	$a = 4.007$	$a = 3.983$[b]	+0.6
		$b = 3.831$	$b = 3.826$	+0.1
		$c = 12.964$	$c = 12.790$	+1.4
		$\beta = 90.607°$	$\beta = 90.750°$	−0.2
NbO_2	Tetragonal ($I41/aZ$)	$a = 13.740$	$a = 13.660$[c]	+0.6
		$c = 6.030$	$c = 5.964$	+1.1
NbO	Cubic ($Pm\bar{3}m$)	$a = 4.223$	$a = 4.211$[d]	+0.3
Ag	Cubic ($Fm\bar{3}m$)	$a = 4.113$	$a = 4.086$[e]	+0.7
Nb	Cubic ($Im\bar{3}m$)	$a = 3.312$	$a = 3.300$[f]	+0.4
O_2	Monoclinic ($C2/m$)	$a = 5.403$	$a = 5.403$[g]	
		$b = 3.429$	$b = 3.429$	
		$c = 5.086$	$c = 5.086$	
		$\beta = 132.530°$	$\beta = 132.530°$	

Oxygen-molecular crystal, the theoretical lattice parameter was fixed to the experimental value.
[a] ICSD #35540 (unknown). [b] ICSD #25765 (unknown). [c] ICSD #28500 (298 K). [d] ICSD #40318 (unknown). [e] ICSD #64994 (291 K). [f] ICSD #76554 (293 K). [g] ICSD #18311 (23 K).

Table 3. Bond angles and interatomic distances of various $AgNbO_3$ phases.

Crystal system	Space group	Bond angles (°)	Interatomic distances (Å)	
		(Nb—O—Nb)	(Nb—O)	(Ag—O)
Cubic	$Pm\bar{3}m$	180.000 [× 6][a]	1.989 [× 6][b]	2.813 [× 12][b]
Tetragonal	*P4/mbm*	180.000 [× 2] *z* 158.286 [× 4]	1.989 [× 2] *z* 2.003 [× 4]	2.546[× 4], 3.074[× 4] 2.782 [× 4]
Orthorhombic	*Cmcm*	165.457 [× 2] *z* 160.661 [× 2] *y* 156.516 [× 2] *x*	1.997 [× 2] *z* 2.002 [× 2] *y* 2.003 [× 2] *x*	2.420 [× 2], 3.024 [× 2] 2.545 [× 2], 3.034 [× 4] 2.749 [× 2]
	Pbcm	163.302, 151.095 *x* 163.302, 151.095 *y* 157.447, 155.180 *z* (O—Nb—O) 171.920 *x* 171.835 *y* 165.222 *z*	1.872, 2.194 1.878, 2.214 1.997 [× 2] *z*	2.403, 2.892 [× 2] 2.416 [× 2], 3.150 [× 2] 2.765 [× 2], 3.149 2.863 [× 2]
	$Pc21b^{VP}$	158.747, 157.051 *y* 157.241, 155.923 157.241, 155.923 (O—Nb—O) 171.377, 169.816 *y* 169.190, 168.983 *x* 168.989, 169.014 *z*	1.885, 2.172 *y* 1.901, 2.136 1.901, 2.145 (× 4)[c] 1.887, 2.174 *y* 1.895, 2.145 1.895, 2.146 (× 4)	2.412, 2.421, 2.427, 2.717, 2.739, 2.750, 2.951, 2.960, 2.986, 3.137, 3.155 [× 2] (× 4)[c] 2.424 [× 2], 2.500, 2.725, 2.729, 2.760, 2.833, 2.884, 2.972, 3.126, 3.158, 3.243 (× 4)
Rhombohedral	$R3cR^{VP}$	156.501 [× 9] *x*, *y*, *z* 156.500 [× 3] *x*, *y*, *z* (O—Nb—O) 169.096 [× 18] *x*, *y*, *z* 169.095 [× 6] *x*, *y*, *z*	1.890 [× 3] *x*, *y*, *z* 2.162 [× 3] *x*, *y*, *z*	2.417 [× 4] 2.741 [× 4] 2.974 [× 4]

VP: Virtual phase.
[a] Numbers of bond angles in a unit cell. [b] Coordination number of O atom in a unit cell. [c] Set of bond length in a unit cell.

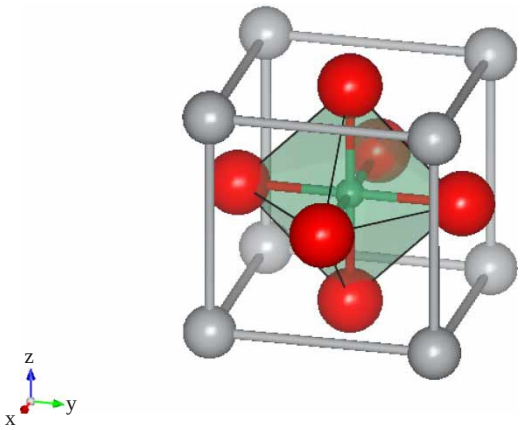

Figure 1. Schematic view of a primitive lattice of a typical perovskite structure. Grey, red and green balls denote silver (Ag^{1+}), oxygen (O^{2-}) and niobium (Nb^{5+}) ions, respectively (see online version for colour). Semi-transparent display areas in green colour denote oxygen octahedrons.

$Pc2_1b^{VP}$) and rhombohedral ($R3cR^{VP}$) phases gives rise to a three-dimensional distortion of the oxygen octahedron in the direction towards *X*-, *Y*- and *Z*-axes. Note that the axes of three-dimensional coordinate, i.e. *X*-, *Y*- and *Z*-axes, which denote the directions from a Nb atom towards O atoms in the oxygen octahedron, will not necessarily be the same as the axes of crystalline lattice, i.e. *a*-, *b*- and *c*-axes. The structures of various phases of $AgNbO_3$ are shown in Figure 2. The Nb atom medially located in an oxygen octahedron is in the symmetry centre of the cubic ($Pm\bar{3}m$), tetragonal (*P4/mbm*) and orthorhombic (*Cmcm*) phases, while the medial Nb atom in the orthorhombic (*Pbcm*), orthorhombic ($Pc2_1b^{VP}$) and rhombohedral ($R3cR^{VP}$) phases differs from the location of the symmetry centre. Consequently, although $AgNbO_3$ in the cubic ($Pm\bar{3}m$), tetragonal (*P4/mbm*) and orthorhombic (*Cmcm*) phases cannot give rise to dielectric polarisation, $AgNbO_3$ in the orthorhombic (*Pbcm*), orthorhombic ($Pc2_1b^{VP}$) and rhombohedral ($R3cR^{VP}$) phases can undergo spontaneous polarisation.

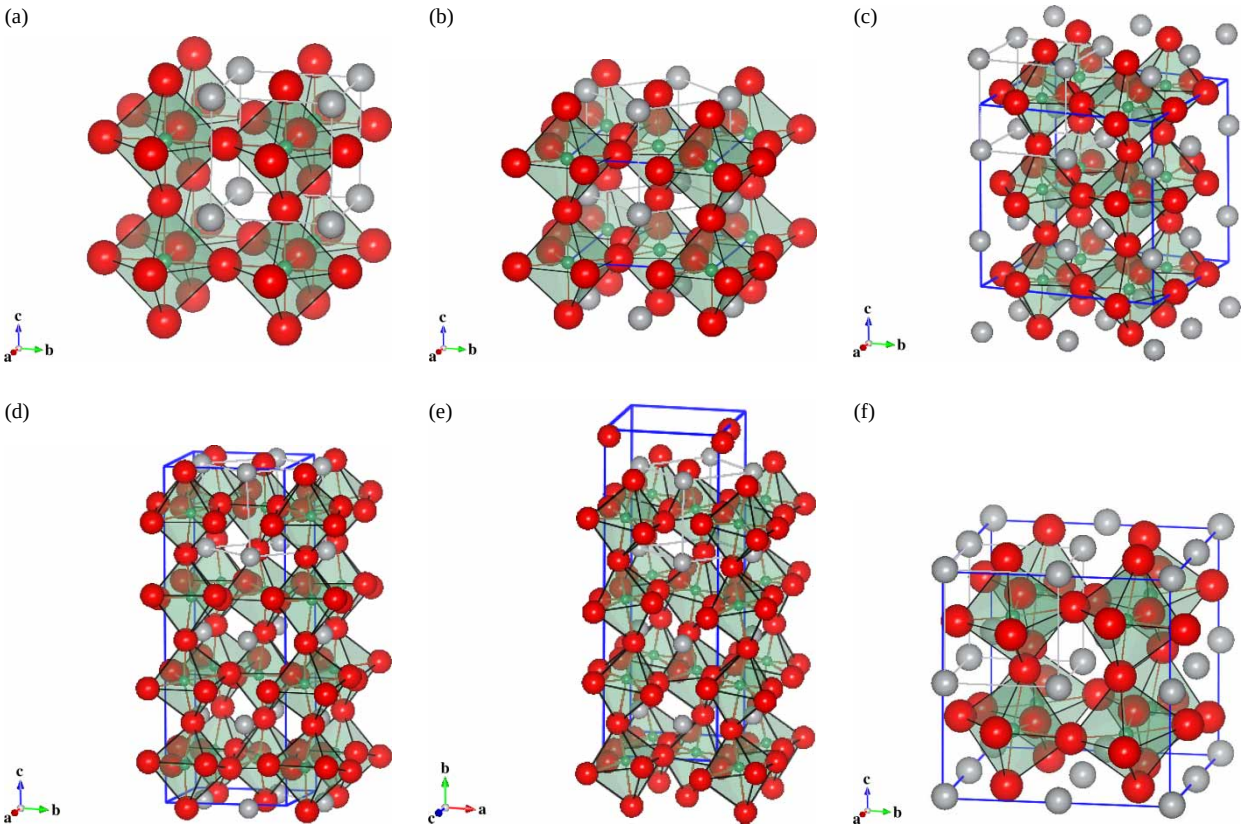

Figure 2. Various phases of $AgNbO_3$. Label axes denote the axes of crystalline lattice. A blue line denotes a unit cell of each phase of $AgNbO_3$ (see online version for colour). (a) Cubic phase ($Pm\bar{3}m$), (b) tetragonal phase ($P4/mbm$), (c) orthorhombic phase ($Cmcm$), (d) orthorhombic phase ($Pbcm$), (e) orthorhombic phase ($Pc2_1b$) and (f) rhombohedral phase ($R3cR$).

3.2 *Formation enthalpy*

The formation enthalpy at 0 K, i.e. H^0, equals the internal energy U. The formation enthalpy at the temperature T, i.e. H^T, can be expressed as

$$H^T = H^0 + \int_0^T C_p \mathrm{d}T, \tag{1}$$

where C_p is the heat capacity at constant pressure. The formation enthalpy at T for $AgNbO_3$ can be expressed as

$$\begin{aligned}
&\Delta H_f^T(AgNbO_3) \\
&= H^T(AgNbO_3) - H^T(Ag) - H^T(Nb) - 3H^T(O) \\
&= \Delta H_f^0(AgNbO_3) + \int_0^T [C_p(AgNbO_3) \\
&\quad - C_p(Ag) - C_p(Nb) - 3C_p(O)]\mathrm{d}T \\
&\approx \Delta H_f^0(AgNbO_3) = \Delta U(AgNbO_3) \\
&= E_t(AgNbO_3) - [E_t(Ag) + E_t(Nb) + 3E_t(O)],
\end{aligned} \tag{2}$$

where ΔH_f is the formation enthalpy, ΔU is the internal energy variation and E_t is the total energy of the compound per formula unit. In the solid, the heat capacity of a chemical compound can be approximated by the sum of the heat capacities of its constituent elements according to the Neumann–Knopp law [29]. In the present case, since the $C_p(AgNbO_3)$ is nearly equal to the sum of $C_p(Ag)$, $C_p(Nb)$ and $3C_p(O)$, the heat capacity terms in Equation (2) are considered to be zero. Therefore, the formation enthalpy at T for $AgNbO_3$ can be expressed approximately as $\Delta U(AgNbO_3)$. In this study, the theoretical and experimental formation enthalpies for Ag_2O, NbO, NbO_2, Nb_2O_5 and various $AgNbO_3$ phases are shown in Table 4 [30]. The theoretical formation enthalpies of Ag_2O and the niobium oxides such as NbO, NbO_2, and Nb_2O_5 are in good agreement with their experimental values within an error of $\pm 2\%$. Thus, the formation enthalpy at 0 K obtained from the present theoretical calculation agrees with the experimental standard enthalpy change of formation at 298 K, since the contribution of internal energy at 0 K is dominant and the contribution of heat capacity can be disregarded.

The theoretical value for cubic $AgNbO_3$ phase is estimated to be -941.6 kJ/mol. We previously reported that the theoretical values for the cubic $NaNbO_3$ and for the hexagonal $LiNbO_3$ phases, i.e. $\Delta H(NaNbO_3)$ and $\Delta H(LiNbO_3)$ were -1291.5 and -1327.7 kJ/mol, respectively, which agreed with the experimental formation

Table 4. Theoretical and experimental formation enthalpies for Ag_2O, NbO, NbO_2, Nb_2O_5 and various $AgNbO_3$ phases.

Compounds (space group)	Formation enthalpies (kJ/mol) Theoretical	Experimental	Error (%)
Ag_2O ($Pn\bar{3}mS$)	− 30.9	− 31.1[a]	+0.6
NbO ($Pm\bar{3}m$)	− 415.9	− 419.7[a,b]	+0.9
NbO_2 ($I41/aZ$)	− 785.0	− 795.0[a]	+1.3
Nb_2O_5 ($A2/m$)	− 1926.8	− 1899.5[a]	− 1.4
$AgNbO_3$ ($Pm\bar{3}m$)	− 941.6		
($P4/mbm$)	− 949.4		
($Cmcm$)	− 950.2		
($Pbcm$)	− 956.1		
$(Pc2_1b)^{VP}$	− 955.8		
$(R3cR)^{VP}$	− 956.4		

1 eV = 96.485 kJ/mol. VP: Virtual phase.
[a] Ref. [30].
[b] Hexagonal phase.

enthalpies [30,31] within an error of ±3%. From this fact, we consider the theoretical formation enthalpies of $AgNbO_3$ are reliable to the same level of accuracy.

The theoretical formation enthalpy for the $AgNbO_3$ decreases with decreasing crystal symmetry. Although the orthorhombic (*Pbcm*) phase with lower symmetry has the lowest formation enthalpy among the physically realised phases, the virtual rhombohedral (*R3cR*) phase with the lowest symmetry has the lowest formation enthalpy among all phases. In light of formation enthalpies, the rhombohedral phase of $AgNbO_3$ is most stable at low temperatures. From this result, we speculate that the rhombohedral (*R3cR*) phase may exist at extremely low temperatures.

3.3 *Electronic structure of $AgNbO_3$*

3.3.1 *Electronic structure of cubic phase*

We first examine the electronic structure of cubic $AgNbO_3$. The band structure and total (T) and local (L) DOS for cubic $AgNbO_3$ are shown in Figure 3. The assignments of the valence band were performed using LDOS and partial (P) DOS. The lower half of the valence band within the energy range from − 6 to − 3 eV mainly consists of the bonding orbital (the so-called e_g orbital) of O 2p and Nb 4d, and the upper half of the valence band within the energy range from − 3 to 0 eV consists of the localised Ag 4d and O 2p components. It is found that the electrons of Ag 4d orbital are localised in the energy area about − 1.5 eV, due to the linear band dispersion of the overall Brillouin zone. On the other hand, the lower half of the conduction band within the energy range from 2.5 to 6 eV mainly consists of antibonding orbitals (the so-called e_g^* orbital) of Nb 4d and O 2p under the Ag 5s components, and the bottom of the conduction band around 2 eV mainly consists of a nonbonding orbital (the so-called t_{2g} orbital) that arises from Nb 4d components. The electronic structures of $AgNbO_3$ characterised by the localised Ag 4d lie at about − 1.5 eV, and play little role in the bonding of the O atoms.

The band structure and TDOS and LDOS for cubic $NaNbO_3$ are shown in Figure 4 for reference. In normal perovskite compounds such as $NaNbO_3$, i.e. in the perovskite compounds having an A-site atom without d orbital electrons, the top of the valence band consists of only O 2p components, and the orbital component of Na at A-site does not appear in the valence band. In this case, the chemical bonding between the Na 3s and O 2p orbitals is ionic while the chemical bonding between Nb 4d and O 2p

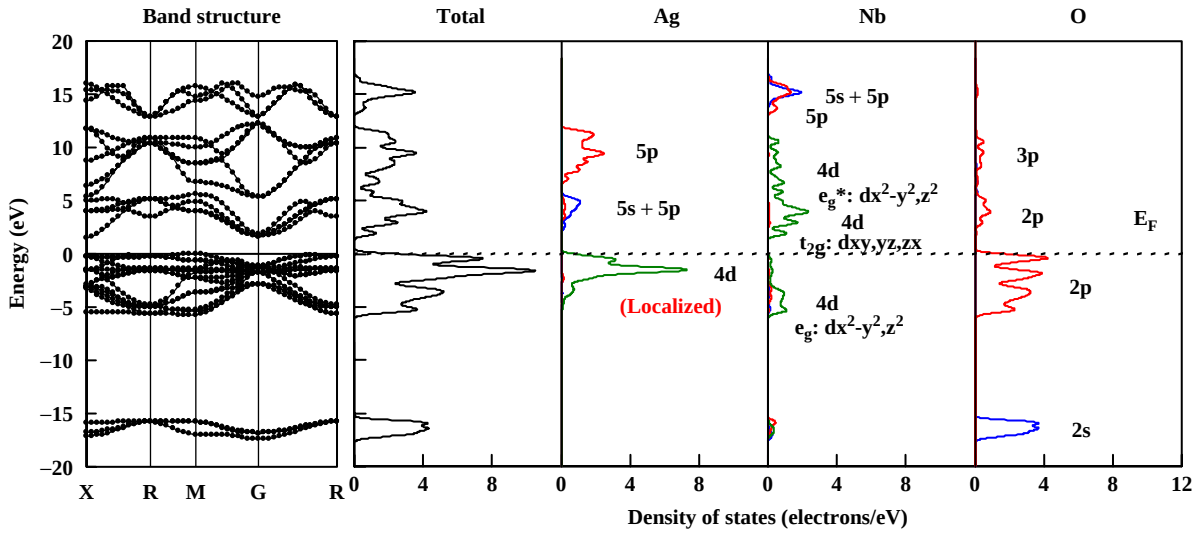

Figure 3. Band structure and TDOS and LDOS for cubic $AgNbO_3$. Black, blue, red and green lines in DOS denote total, s, p and d components, respectively (see online version for colour).

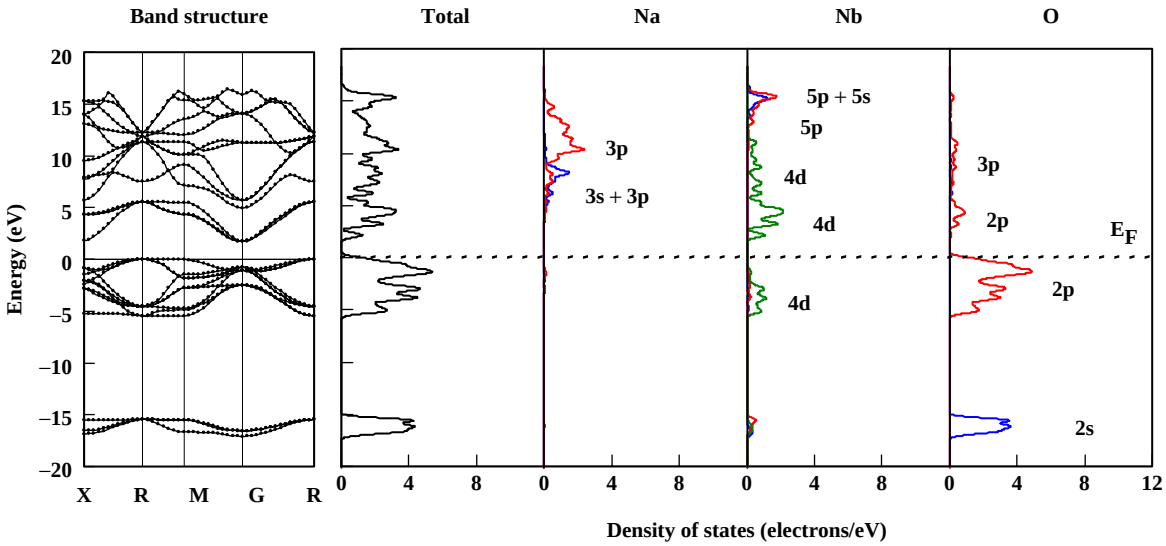

Figure 4. Band structure and TDOS and LDOS for cubic $NaNbO_3$. Black, blue, red and green lines in DOS denote total, s, p and d components, respectively (see online version for colour).

orbitals is partially covalent. On the other hand, even though the Ag 4d and O 2p components in $AgNbO_3$ lie in the valence band, the filled Ag 4d electrons may affect on the bonding of the O atoms. Therefore, the chemical bonding between Ag and O atoms becomes ionic with some covalent component and the chemical bonding between the Nb 4d and O 2p orbitals is partially covalent.

The assignments of theoretical DOS for $AgNbO_3$ and $NaNbO_3$ account nicely for the experimental results of X-ray photoelectron spectroscopy (XPS) measured by Kruczek et al. [32], i.e. the valence band of $AgNbO_3$ is formed mainly of the Nb 4d, Ag 4d and O 2p states, while that of $NaNbO_3$ consist of the O 2p states hybridised with the Nb 3d states.

3.3.2 *Density of states of various phases*

We next studied the electronic structures of the various phases of $AgNbO_3$ using GGA-PBE exchange-correlation functions [8,25]. The TDOS and PDOS for the various $AgNbO_3$ phases are shown in Figure 5. The assignments of the valence band were performed employing the same procedure as used for Figure 3. The experimental band gap of $AgNbO_3$ estimated from the XPS measurements by Kruczek et al. [32] is about 3 eV [32]. On the other hand, the theoretical band gap of the real anti-ferroelectric phase (*Pbcm*) in $AgNbO_3$ is 1.95 eV at 0 K by our calculation. Note that this phase is observed at room temperature. Thus, the theoretical value of the band gap for $AgNbO_3$ is underestimated due to using the GGA-PBE exchange-correlation functions [8,25] on the basis of density functional theory in the present work.

When the symmetry of the crystal system in $AgNbO_3$ decreases, the bonding and anti-bonding orbitals (especially Nb—O) separate, due to the presence of long and short bonds by the change of Nb—O length as can be seen from Table 3. This phenomenon is well known as Peierls distortion [33] or Jahn–Teller effect in solid state [34,35] which the energy of the crystal system stabilises, since the degeneracy of these orbitals is lifted due to the phase transition to lower symmetry. In the real anti-ferroelectric phase (*Pbcm*) and the virtual ferroelectric phases ($Pc2_1b$, $R3cR$), the change in the Nb—O length is very large. Consequently, the band gaps of these phases with the lower symmetry are widening in comparison to the paraelectric phases ($Pm\bar{3}m$, *P*4/*mbm* and *Cmcm*) with higher symmetry. The theoretical values of the band gaps for $Pm\bar{3}m$, *P*4/*mbm*, *Cmcm*, *Pbcm*, $Pc2_1b$ and $R3cR$ phases are 1.51, 1.18, 1.20, 1.95, 2.11 and 2.30 eV, respectively. Here, we become aware that the theoretical band gaps of the tetragonal (*P*4/*mbm*) and orthorhombic (*Cmcm*) phases are narrower than that of cubic ($Pm\bar{3}m$) phase. When the symmetry of the crystal system in $AgNbO_3$ decreases from cubic to the other systems, the localised electrons of the Ag 4d orbitals become delocalised due to the presence of short bonds by a substantial change in the Ag—O atomic distance as can be seen from Table 3, and the Ag 4d orbitals on the bonding orbital of O 2p—Nb 4d widen due to interaction with the O 2p electrons. As a result, the theoretical values of the band gaps for the *P*4/*mbm* and *Cmcm* phases narrow in comparison to that of the $Pm\bar{3}m$ phase. Note that the conduction band bottom (CBB) for the *P*4/*mbm* and *Cmcm* phases appears to decrease, since the energy level of the valence band top is set to 0 eV [= Fermi energy (E_F)] in this study.

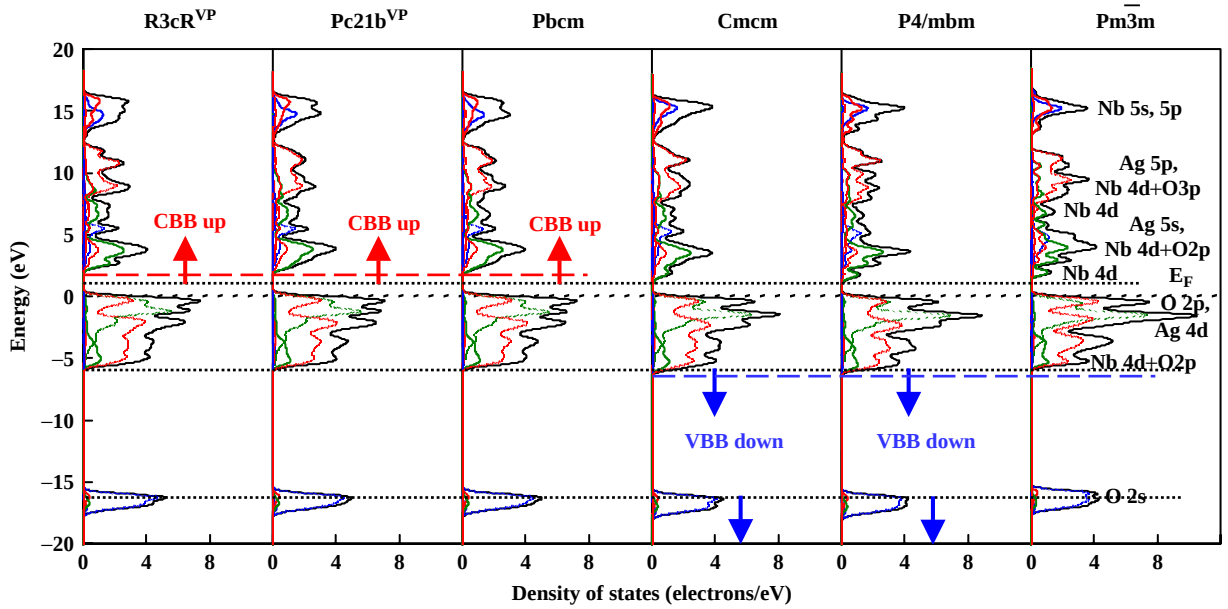

Figure 5. TDOS and PDOS for various $AgNbO_3$ phases. Black, blue, red and green lines denote total, s, p and d components, respectively (see online version for colour). CBB, valence band bottom (VBB). Note that the CBB and VBB for *P*4/*mbm* and *Cmcm* phases appear to be decreasing in comparison with those for $Pm\bar{3}m$ phase, since the energy level of valence band top is set to 0 eV ($= E_F$) in this study.

In order to investigate the influence of the Ag 4d orbitals, we determined the electronic structures of the various phases of $NaNbO_3$ within the GGA-PBE exchange-correlation functional [8,25]. The TDOS and PDOS for the various $NaNbO_3$ phases are shown in Figure 6. The experimental band gap of $NaNbO_3$ as well as $AgNbO_3$ is about 4 eV [32]. On the other hand, the theoretical band gap of the anti-ferroelectric phase (*Pbma*) in $NaNbO_3$ is 2.48 eV at 0 K by our calculation. Note that this phase is observed at room temperature. The theoretical value of the band gap of $NaNbO_3$ is underestimated again. However, the trend in band gap width is correct, i.e. the band gap of $AgNbO_3$ is narrower than that of $NaNbO_3$, consistent with the experimental results of Kruczek et al. [32].

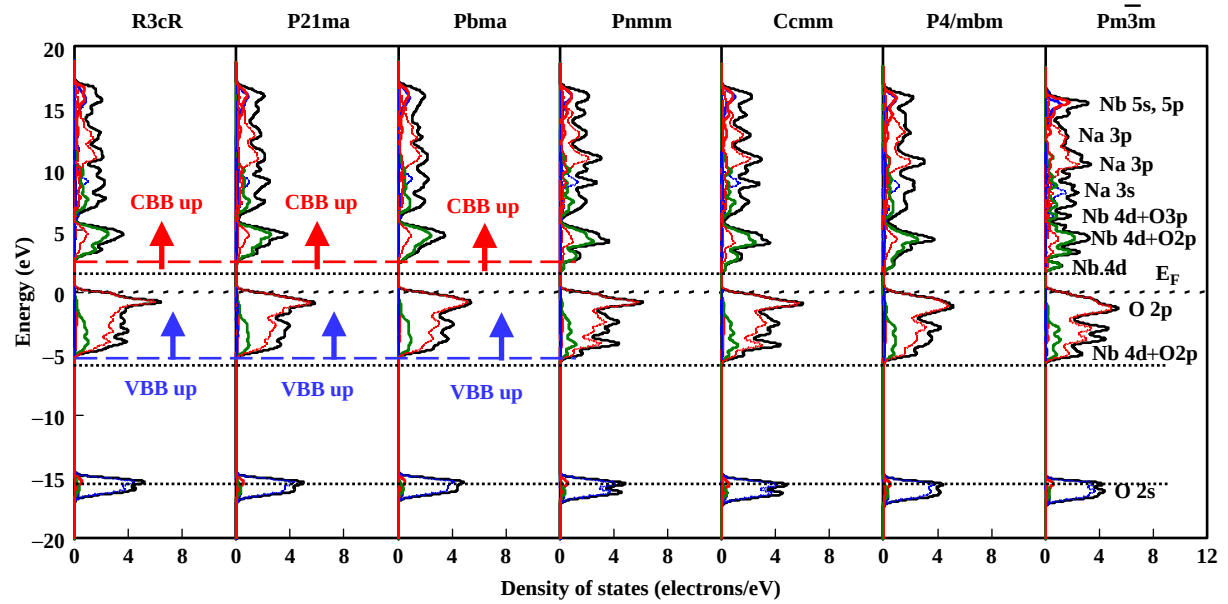

Figure 6. TDOS and PDOS for various $NaNbO_3$ phases. Black, blue, red and green lines denote total, s, p and d components, respectively (see online version for colour). CBB, VBB.

When the symmetry of the crystal system in $NaNbO_3$ decreases, the bonding and anti-bonding orbitals repel, due to the presence of long and short bonds leading to a change in Nb—O length similar to $AgNbO_3$. In the anti-ferroelectric (*Pbma*) and the ferroelectric phases ($P2_1ma$, *R*3*cR*), the change in the Nb—O bond length is very large. Consequently, the band gaps of these phases with the lower symmetry widen in comparison to the paraelectric phases ($Pm\bar{3}m$, *P*4/*mbm*, *Ccmm* and *Pnmm*) with higher symmetry. The theoretical values of the band gaps for the $Pm\bar{3}m$, *P*4/*mbm*, *Ccmm*, *Pnmm*, *Pbma*, $P2_1ma$ and *R*3*cR* phases are 1.71, 1.73, 1.84, 1.95, 2.48, 2.50 and 2.92 eV, respectively. In $NaNbO_3$, the band gaps of the paraelectric phases widen in turn from the $Pm\bar{3}m$ to the *Pnmm* phase in sharp contrast with $AgNbO_3$. When the symmetry of the crystal system in $NaNbO_3$ decreases from cubic to other system, the interaction between Na and O is small compared to that between Ag and O in $AgNbO_3$, since there is no Na component of the valence band. As a consequence, the trend in the theoretical band gaps among the paraelectric phases of $AgNbO_3$ differs considerably from that of $NaNbO_3$.

4. Summary

In order to evaluate the phase stability for all the real $AgNbO_3$ phases ($Pm\bar{3}m$, *P*4/*mbm*, *Cmcm* and *Pbcm*) that appear under atmospheric pressure and for the virtual phases ($Pc2_1b$ and *R*3*cR*), which are observed in $NaNbO_3$, we obtained the formation enthalpies of the various $AgNbO_3$ phases using a plane-wave pseudopotential method [7]. Although the orthorhombic (*Pbcm*) phase with the lower symmetry has the lowest formation enthalpy among the real phases, the virtual rhombohedral (*R*3*cR*) phase with the lowest symmetry has the lowest formation enthalpy among all phases. In the light of its low formation enthalpy, we speculate that the rhombohedral (*R*3*cR*) phase may exist at extremely low temperatures.

We have studied the electronic structures of the various phases of $AgNbO_3$ within the GGA-PBE exchange-correlation functional [8,25]. The assignments of the valence band were performed using LDOS and PDOS. The valence band top consists of localised Ag 4d and O 2p orbitals along with the bonding orbital of O 2p—Nb 4d, while the lower conduction band mainly consists of the anti-bonding orbital of Nb 4d—O 2p below the Ag 5s orbital for all phases. When the symmetry of the crystal system in $AgNbO_3$ decreases, these orbitals (especially Nb—O) repel, hence the band gaps of the virtual ferroelectric phases ($Pc2_1b$ and *R*3*cR*) and the real anti-ferroelectric phase (*Pbcm*) with the lower symmetry widen in comparison to the paraelectric phases ($Pm\bar{3}m$, *P*4/*mbm* and *Cmcm*) with the higher symmetry.

We have also investigated the relationship between the electronic structure and structural distortion in $AgNbO_3$. When the symmetry of the crystal system in $AgNbO_3$ decreases, the total energy of the system is decreased by tilting of the oxygen octahedron, and the energy change depends in large measure on the tilt angle. Although the theoretical band gaps of the paraelectric phases with distortions are smaller than that of the cubic phase, the total energies of these systems decrease by the tilting of oxygen octahedrons. In contrast, the theoretical band gaps of the anti-ferroelectric and ferroelectric phases are wider than those of all the paraelectric phases due to a shift to lower energies of the Nb—O bonding orbital in the valence band and the shift to higher energies of the Nb—O antibonding orbital in the conduction band. Therefore, the large distortion and the Nb—O short bond in $AgNbO_3$ lower the symmetry and decrease the total energies of the anti-ferroelectric and ferroelectric phases.

Acknowledgements

The authors are grateful to Dr H. Moriwake of Japan Fine Ceramics Center, for helpful advice. The authors would also like to thank Dr Y. Matsuo, Mr T. Maeda, Mr T. Koyama and Mr T. Yamamoto of the Department of Materials Chemistry, Ryukoku University, for profitable arguments. The authors would also like to thank Dr P. Fons of the National Institute of Advanced Industrial Science and Technology for his critical reading of the manuscript.

Note

1. Email: twada@rins.ryukoku.ac.jp

References

[1] K. Uchino, *Ferroelectric Devices*, Marcel Dekker, Inc., New York, NY, 2000, pp. 1–22, 145–220.
[2] Y. Saito, H. Takao, T. Tani, T. Nonoyama, K. Takatori, T. Homma, T. Nagaya, and M. Nakamura, *Lead-free piezoceramics*, Nature 432 (2004), pp. 84–87.
[3] A. Shigemi and T. Wada, *Enthalpy of formation of various phases and formation energy of point defects in perovskite-type $NaNbO_3$ by first-principles calculation*, Jpn. J. Appl. Phys. 43 (2004), pp. 6793–6798.
[4] A. Shigemi and T. Wada, *Evaluations of phases and vacancy formation energies in $KNbO_3$ by first-principles calculation*, Jpn. J. Appl. Phys. 44 (2005), pp. 8048–8054.
[5] A. Shigemi and T. Wada, *First-principles studies of phase stability and the neutral atomic vacancies in $LiNbO_3$, $NaNbO_3$ and $KNbO_3$,* in *Ferroelectric Thin Films XIII*, R. Ramesh, J.-P. Maria, M. Alexe, and V. Joshi, eds., Mater. Res. Soc. Symp. Proc. 902E (2006), Warrendale, PA, 0902-T10-46.
[6] A. Shigemi, T. Koyama, and T. Wada, *First-principles studies of various crystallographic phases and neutral atomic vacancies in $KNbO_3$ and $KTaO_3$*, Phys. Stat. Sol. (c) 3 (2006), pp. 2862–2866.
[7] M.D. Segall, P.J.D. Lindan, M.J. Probert, C.J. Pickard, P.J. Hasnip, S.J. Clark, and M.C. Payne, *First-principles simulation: ideas, illustrations and the CASTEP code*, J. Phys.: Cond. Matter. 14 (2002), pp. 2717–2744.
[8] J.P. Perdew, J.A. Chevary, S.H. Vosko, K.A. Jackson, M.R. Pederson, D.J. Singh, and C. Fiolhais, *Atoms, molecules, solids, and surfaces: applications of the generalized gradient approximation for exchange and correlation*, Phys. Rev. B 46 (1992), pp. 6671–6687.

[9] Y. Shiozaki, E. Nakamura, and T. Mitsui, *Landolt-Börnstein*, vol. III/36A1, Springer-Verlag, Berlin, Heidelberg, New York, 2001, p. 67.

[10] M. Valant and D. Suvorov, *New high-permittivity $AgNb_{1-x}Ta_xO_3$ microwave ceramics: Part II, dielectric characteristics*, J. Am. Ceram. Soc. 82 (1999), pp. 88–93.

[11] M.H. Francombe and B. Lewis, *Structural and electrical properties of silver niobate and silver tantalate*, Acta Crystallogr. 11 (1958), pp. 175–178.

[12] A. Kania and J. Kwapulinski, *$Ag_{1-x}Na_xNbO_3$ (ANN) solid solutions: from disordered antiferroelectric $AgNbO_3$ to normal antiferroelectric $NaNbO_3$*, J. Phys.: Condens. Matter. 11 (1999), pp. 8933–8946.

[13] A. Kania, *Dielectric properties of $Ag_{1-x}A_xNbO_3$ (A: K, Na and Li) and $AgNb_{1-x}Ta_xO_3$ solid solutions in the vicinity of diffuse phase transitions*, J. Phys. D 34 (2001), pp. 1447–1455.

[14] A. Kania and S. Miga, *Preparation and dielectric properties of $Ag_{1-x}Li_xNbO_3$ (ALN) solid solutions ceramics*, Mater. Sci. Eng. B 86 (2001), pp. 128–133.

[15] Ph. Sciau, A. Kania, B. Dkhil, E. Suard, and A. Ratuszna, *Structural investigation of $AgNbO_3$ phases using x-ray and neutron diffraction*, J. Phys.: Condens. Matter. 16 (2004), pp. 2795–2810.

[16] D. Fu, M. Endo, H. Taniguchi, T. Taniyama, and M. Itoh, *$AgNbO_3$: a lead-free material with large polarization and electromechanical response*, Appl. Phys. Lett. 90 (2007), 252907.

[17] Y. Sakabe, T. Takeda, Y. Ogino, and N. Wada, *Ferroelectric properties of (Ag,Li)(Nb,Ta)O_3 ceramics*, Jpn. J. Appl. Phys. 40 (2001), pp. 5675–5678.

[18] S. Wada, A. Saito, T. Hoshina, H. Kakemoto, T. Tsurumi, C. Moriyoshi, and Y. Kuroiwa, *Growth of large-scale silver lithium niobate single crystals and their piezoelectric properties*, Jpn. J. Appl. Phys. 45 (2006), pp. 7389–7396.

[19] H.J. Monkhorst and J.D. Pack, *Special points for Brillouin-zone integrations*, Phys. Rev. B 13 (1976), pp. 5188–5192.

[20] D. Vanderbilt, *Soft self-consistent pseudopotentials in a generalized eigenvalue formalism*, Phys. Rev. B 41 (1990), pp. 7892–7895.

[21] G. Kresse and J. Furthmüller, *Efficient iterative schemes for* ab initio *total-energy calculations using a plane-wave basis set*, Phys. Rev. B 54 (1996), pp. 11169–11186.

[22] M.C. Payne, M.P. Teter, D.C. Allan, T.A. Arias, and J.D. Joannopoulos, *Iterative minimization techniques for* ab initio *total-energy calculations: molecular dynamics and conjugate gradients*, Rev. Mod. Phys. 64 (1992), pp. 1045–1097.

[23] W.H. Press, S.A. Teukolsky, W.T. Vetterling, and B.P. Flannery, *Numerical Recipes*, 2nd ed., Cambridge University Press, Cambridge, 1992, p. 418.

[24] C.S. Barrett, L. Meyer, and J. Wasserman, *Antiferromagnetic and crystal structures of alpha-oxygen*, J. Chem. Phys. 47 (1967), pp. 592–597.

[25] J.P. Perdew, K. Burke, and M. Ernzerhof, *Generalized gradient approximation made simple*, Phys. Rev. Lett. 77 (1996), pp. 3865–3868.

[26] R. von der Muehll, A. Sadel, and P. Hagenmuller, *Structure cristallinea 295 K de la phase ferroelectrique $Li_{0.02}Na_{0.98}NbO_3$*, J. Solid State Chem. 51 (1984), pp. 176–182.

[27] P. Seidel and W. Hoffmann, *Golden Book of Phase Transitions*, vol. 1, Wroclaw, Poland, 2002, pp. 1–123.

[28] R.D. Shannon, *Revised effective ionic radii and systematic studies of interatomic distances in halides and chalcogenides*, Acta Crystallogr. A 32 (1976), pp. 751–767.

[29] O. Kubaschewski, C.B. Alcock, and P.J. Spencer, *Materials Thermochemistry*, 6th ed., Pergamon Press, Oxford, 1993, p. 167.

[30] O. Kubaschewski, C.B. Alcock, and P.J. Spencer, *Materials Thermochemistry*, 6th ed., Pergamon Press, Oxford, 1993, p. 257.

[31] I. Pozdnyakova, A. Navrotsky, L. Shilkina, and L. Reznitchenko, *Thermodynamic and structural properties of sodium lithium niobate solid solutions*, J. Am. Ceram. Soc. 85 (2002), pp. 379–384.

[32] M. Kruczek, E. Talik, and A. Kania, *Electronic structure of $AgNbO_3$ and $NaNbO_3$ studied by X-ray photoelectron spectroscopy*, Solid State Commun. 137 (2006), pp. 469–473.

[33] R.E. Peierls, *Quantum Theory of Solids*, Oxford University Press, Oxford, 1972.

[34] H.A. Jahn and E. Teller, *Stability of polyatomic molecules in degenerate electronic states. 1. Orbital degeneracy*, Proc. Roy. Soc. A161 (1937), pp. 220–235.

[35] R.A. Wheeler, M.-H. Whangbo, T. Hughbanks, R. Hoffmann, J.K. Burdett, and T.A. Albright, *Symmetric vs. asymmetric linear M-X-M linkages in molecules, polymers, and extended networks*, J. Am. Chem. Soc. 108 (1986), pp. 2222–2236.